

## Two Types of Charge Ordering in the Half-Doped Manganites of $\text{Bi}_{0.5}(\text{Ca,Sr})_{0.5}\text{MnO}_3$

Yoichi HORIBE<sup>1</sup>, Jai-Seok AHN<sup>1,2\*</sup>, Peter A. SHARMA<sup>1†</sup>, Shigeo MORI<sup>3</sup>,  
Cheng-Hsuan CHEN<sup>4</sup>, Se-Jung OH<sup>2</sup>, and Sang-Wook CHEONG<sup>1‡</sup>

<sup>1</sup>Rutgers Center for Emergent Materials and Department of Physics and Astronomy, Rutgers University,  
Piscataway, NJ 08854, U.S.A.

<sup>2</sup>School of Physics and Center for Strongly Correlated Materials Research, Seoul National University,  
Seoul 151-742, Republic of Korea

<sup>3</sup>Department of Materials Science, Osaka Prefecture University, Osaka 599-8531

<sup>4</sup>Center for Condensed Matter Sciences, National Taiwan University, Taipei 101, Taiwan

(Received November 6, 2008; accepted January 27, 2009; published March 25, 2009)

From our study of the evolution of charge ordering in  $\text{Bi}_{0.5}\text{Ca}_{0.5-x}\text{Sr}_x\text{MnO}_3$  ( $x = 0-0.5$ ) with chemical pressure, we found the detailed nature of two distinct charge ordering schemes, associated with the structural change from *Pnma*- to *Imma*-type symmetry at  $x = 0.2-0.25$ . Charge ordering for  $x = 0-0.2$  (*Pnma*) is consistent with the checkerboard-type pattern, commonly observed in half-doped manganites. On the other hand, a large tolerance factor for  $x = 0.25-0.5$  (*Imma*) stabilizes a double-stripe charge ordering scheme. These findings indicate the bicritical nature of two competing charge ordered states and provide further insight towards understanding the dominant charge ordering mechanism in half-doped manganites.

KEYWORDS: half-doped manganites, charge ordering, bicritical nature

DOI: [10.1143/JPSJ.78.044704](https://doi.org/10.1143/JPSJ.78.044704)

### 1. Introduction

Charge ordering (CO) in mixed-valent transition metal oxides is a time-honored subject,<sup>1)</sup> and has recently been found to be intriguingly coupled with extraordinary physical phenomena such as the colossal magnetoresistance (CMR) effect in manganites. The CE-type charge ordering in the half-doped manganites with the checkerboard-type (CB) arrangement of  $\text{Mn}^{3+}$  and  $\text{Mn}^{4+}$  ions accompanies orbital as well as spin ordering. Furthermore, the strong interplay between charge, orbital, and the lattice degree of freedom stabilizes charged sheets of  $\text{Mn}^{3+}\text{O}_6$  octahedra with the Jahn–Teller distortion.<sup>2–7)</sup> In  $\text{Ln}_{0.5}\text{Ca}_{0.5}\text{MnO}_3$  ( $\text{Ln} = \text{La}, \text{Pr}, \text{Nd}, \text{Sm}, \text{and Bi}$ ), the CO temperature ( $T_{\text{CO}}$ ) decreases monotonically (from 320 to 160 K) with an increase of the tolerance factor.<sup>8)</sup> This is consistent with the change in bandwidth caused by chemical pressure (or tolerance factor). The ferromagnetic (FM) state is stabilized in  $\text{La}_{0.5}\text{Sr}_{0.5}\text{MnO}_3$  with a large bandwidth, but FM and CO states tend to coexist in  $\text{Nd}_{0.5}\text{Sr}_{0.5}\text{MnO}_3$  and  $\text{Pr}_{0.5}\text{Sr}_{0.5}\text{MnO}_3$  with intermediate bandwidths. Contrary to this general tendency, stable charge ordering ( $T_{\text{CO}} \approx 530$  K) is found in  $\text{Bi}_{0.5}\text{Sr}_{0.5}\text{MnO}_3$ ,<sup>9)</sup> even though  $\text{Bi}^{3+}$  and  $\text{La}^{3+}$  are similar in size.<sup>10)</sup> The extreme stability of CO state in  $\text{Bi}_{0.5}\text{Sr}_{0.5}\text{MnO}_3$  is well indicated by the unusually high  $T_{\text{CO}}$ , which is also remarkably robust against significant Bi-deficiency.<sup>11)</sup> Furthermore, unlike typical wide-band  $\text{Ln}_{0.5}\text{Sr}_{0.5}\text{MnO}_3$ , there is no indication of phase coexistence in  $\text{Bi}_{0.5}\text{Sr}_{0.5}\text{MnO}_3$ . There exist contradictory reports on the nature of CO in  $\text{Bi}_{0.5}\text{Sr}_{0.5}\text{MnO}_3$ . Garcia *et al.* emphasized the importance of the lone pairs of  $\text{Bi}^{3+}$  in  $\text{Bi}_{0.5}\text{Sr}_{0.5}\text{MnO}_3$  and suggested that the larger ionic size with the lone pairs and the covalent Bi–O bonds provide

additional stability of the CO state, based on their structural analysis with *Pnma* cells.<sup>9)</sup> However, Hervieu *et al.* reported a new *Imma*-type structure of  $\text{Bi}_{0.5}\text{Sr}_{0.5}\text{MnO}_3$ , and suggested a new CO scheme as “2+2 double stripe-type (DS)”, consisting of double  $\text{Mn}^{3+}$  sheets alternating with double  $\text{Mn}^{4+}$  sheets.<sup>11)</sup> In fact, the double  $\text{Mn}^{3+}$  sheets, apparently costing a significant Coulombic repulsive energy, are identical to the diagonal  $\text{Mn}^{3+}$  sheets of orbital-ordered  $\text{LaMnO}_3$ . Recent resonant x-ray scattering experiment at the Mn K edge in the CO phase in  $\text{Bi}_{0.5}\text{Sr}_{0.5}\text{MnO}_3$  indicated that the tetragonally distorted and the nearly undistorted  $\text{Mn}^{3+}\text{O}_6$  octahedra coexist in the CO phase of CO in  $\text{Bi}_{0.5}\text{Sr}_{0.5}\text{MnO}_3$ , and as the result, the CB-type CO is a common ground.<sup>12)</sup> In order to further understand these controversial and confusing results, we have studied the detailed CO properties of the mixed system of conventional CB-type  $\text{Bi}_{0.5}\text{Ca}_{0.5}\text{MnO}_3$  and unusual  $\text{Bi}_{0.5}\text{Sr}_{0.5}\text{MnO}_3$ .

In this paper, we report our systematic study of structural, transport, and electron diffraction properties  $\text{Bi}_{0.5}\text{Ca}_{0.5-x}\text{Sr}_x\text{MnO}_3$  ( $x = 0-0.5$ ). We found two different types of CO, which are associated with structural changes between *P*- and *I*-type cells at  $x = 0.2-0.25$ , even though the lattice volume evolves monotonically across the structural boundary. Our measurements systematically indicate the immiscibility of the two different CO schemes and provide insights into understanding the mechanism balancing between these two competing CO phases.

### 2. Experimental

High-quality polycrystalline  $\text{Bi}_{0.5}\text{Ca}_{0.5-x}\text{Sr}_x\text{MnO}_3$  ( $x = 0, 0.05, 0.1, 0.15, 0.2, 0.25, 0.3, 0.35, 0.4, \text{and } 0.5$ ) specimens were used for the present study. The samples were prepared by solid state reaction method with intermediate grinding, and 1100–1150 °C sintering. Specimens were reacted within tightly closed Pt tubes to minimize Bi evaporation. Crystallographic information was obtained from powder x-ray diffraction using the Cu  $K\alpha$  line at room  $T$ . No second phase

\*Present address: Department of Physics, Pusan National University, Pusan 609-735, Republic of Korea.

†Present address: Materials Physics Department, Sandia National Laboratories, MS-9161, Livermore, CA 94551, U.S.A.

‡E-mail: [sangc@physics.rutgers.edu](mailto:sangc@physics.rutgers.edu)

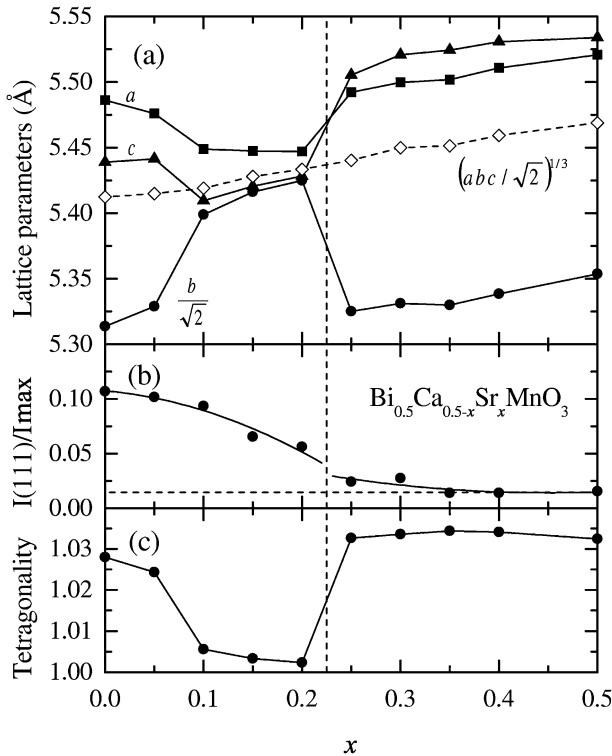


Fig. 1. (a) Orthorhombic lattice parameters and effective lattice-size  $[(abc/\sqrt{2})^{1/3}]$ , (b) Intensity of (111) Bragg reflection normalized with that of (121), and (c) Tetragonality factor  $[(a+c)/\sqrt{2}b]$  of  $\text{Bi}_{0.5}\text{Ca}_{0.5-x}\text{Sr}_x\text{MnO}_3$ .

was detected in the diffraction patterns. DC resistivity was measured with a standard four-probe method at  $T = 10\text{--}800\text{ K}$  and the magnetic properties were measured with a SQUID magnetometer below 400 K. A JEOL 2000 FX transmission electron microscope (TEM) equipped with a low  $T$  stage and a 14-bit charge coupled device (CCD) array detector was used for electron diffractions.

### 3. Results and Discussions

The x-ray diffraction patterns of all specimens were consistent with the distorted perovskite structure that can be indexed with a single orthorhombic cell, i.e.,  $a \cong c \approx \sqrt{2}a_p$  and  $b \approx 2a_p$ , where  $a_p$  is a simple cubic cell parameter. Figure 1(a) shows the refined lattice parameters and the effective lattice size. The monotonic increase of the lattice-size indicates that a homogeneous solid solution is achieved between  $x = 0$  and 0.5. We note that there is no abrupt change of lattice-size as a function of composition, suggesting that the lone pair character of  $\text{Bi}^{3+}$  remains intact in the entire region.<sup>9)</sup> Figure 1(b) depicts the intensity of (111) Bragg reflection. The negligible intensity of (111) for  $x \geq 0.25$  suggests that the average structure for  $x \geq 0.25$  is of the  $Imma$ -type, rather than the common  $Pnma$ -type. Note that the tetragonality factor,  $(a+c)/\sqrt{2}b$  as shown in Fig. 1(c), is larger in the  $I$ -type cell [1.026 ( $x = 0$ ) and 1.032 ( $x = 0.5$ )], and it is close to unity for  $0.1 \leq x \leq 0.2$ . The latter is primarily because CO for  $0.1 \leq x \leq 0.2$  develops below room temperature.

Figure 2 displays the DC resistivity  $\rho(T)$  of  $\text{Bi}_{0.5}\text{Ca}_{0.5-x}\text{Sr}_x\text{MnO}_3$ . Only cooling curves are depicted in the figure for clarity, but we note that significant thermal hysteresis was

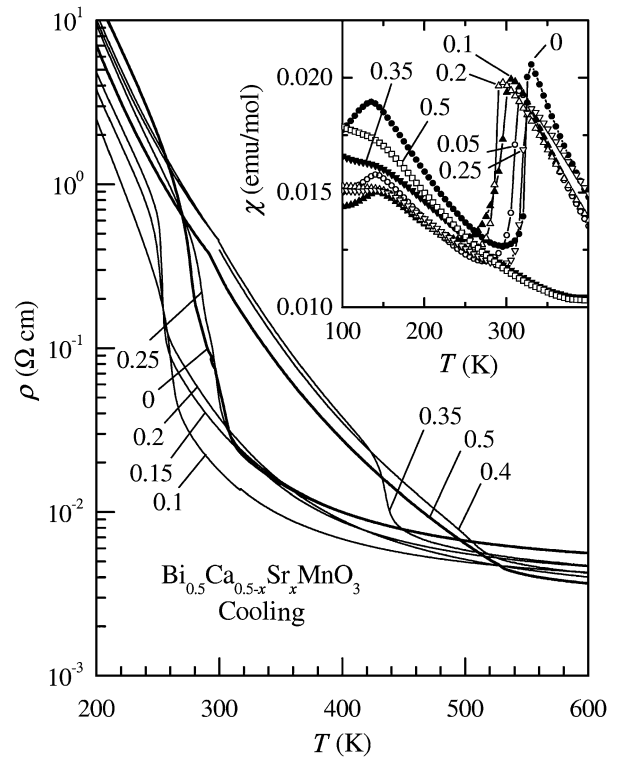


Fig. 2. DC resistivity  $\rho(T)$  of  $\text{Bi}_{0.5}\text{Ca}_{0.5-x}\text{Sr}_x\text{MnO}_3$  upon cooling. Inset: magnetic susceptibility  $\chi(T) (\equiv M/H)$  with applied field  $H = 1000$  ( $x = 0$ ) and 2000 Oe ( $x = 0.05, 0.1, 0.2, 0.25, 0.35, \text{ and } 0.5$ ).  $\chi(T)$  was measured upon warming after zero-field cool to  $T = 5\text{ K}$ .

observed. All the samples exhibit semiconducting behavior, accompanied by the characteristic CO behavior of a significant slope change at  $T_{\text{CO}}$ . The resistivity jump at  $T_{\text{CO}}$  tends to smear out with Sr substitution, but the slope change is still clearly noticeable. The inset shows the magnetic susceptibility,  $\chi(T) \equiv M/H$ . The broad feature of  $\chi(T)$ , starting below about 145 K, results from antiferromagnetic ordering, and the sharp drop of  $\chi(T)$  at higher temperatures signals CO. Note that the drop of  $\chi$  at  $T_{\text{CO}}$  originates from the switching of magnetic correlations from ferromagnetic to antiferromagnetic due to CO.<sup>13)</sup>

Figure 3(a) shows  $T_{\text{CO}}$  and  $T_N$  determined from  $d \ln \rho/dT$  and  $d\chi/dT$ , respectively.  $T_N$  varies little with  $x$ , but  $T_{\text{CO}}$  changes drastically and becomes minimum at  $x = 0.2$ .  $T_{\text{CO}}$  initially decreases with  $x$ , consistent with the increase of tolerance factor. However, for  $x$  above the structural boundary at  $x = 0.2\text{--}0.25$ ,  $T_{\text{CO}}$  sharply increases with  $x$ . Note that this behavior of  $T_{\text{CO}}$  resembles the bicritical nature of two competing, antagonistic ground states.<sup>14)</sup> The details of the CO configurations were studied using TEM. Insets in Fig. 3(a) shows [010] zone-axis typical electron diffraction (ED) patterns obtained from untwinned CO domains of  $\text{Bi}_{0.5}\text{Ca}_{0.5}\text{MnO}_3$  (left) and  $\text{Bi}_{0.5}\text{Sr}_{0.5}\text{MnO}_3$  (right) at room temperature. For  $x = 0$  and 0.05, the fundamental spots are consistent with an orthorhombic  $Pnma$  structure. In addition to the  $Pnma$ -type Bragg peaks, superlattice spots are clearly visible at  $(1/2\ 00)$ -type positions. The superlattice reflections result from the CB-type charge/orbital ordering, characterized by a modulation wave vector,  $\mathbf{q} = \mathbf{a}^*/2$ , where  $\mathbf{a}^*$  is the reciprocal lattice vector along [100] direction. A couple of features in the ED patterns of  $x = 0.35$  and 0.5 are

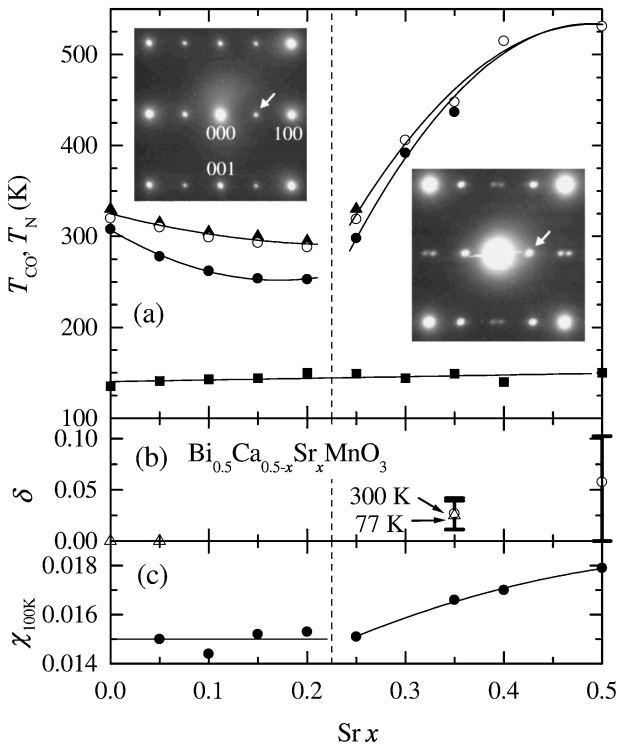


Fig. 3. Compositional dependence of: (a) Charge ordering temperature  $T_{CO}$  (○:  $\rho$  warming, ●:  $\rho$  cooling, and ▲:  $\chi$  warming) and antiferromagnetic ordering temperature  $T_N$  (■) determined from  $d \ln \rho / dT$  and  $d\chi / dT$ , respectively. (b) Incommensurability  $\delta$ . Insets: [010] zone-axis electron diffraction patterns from untwinned CO domains of  $\text{Bi}_{0.5}\text{Ca}_{0.5}\text{MnO}_3$  (left) and  $\text{Bi}_{0.5}\text{Sr}_{0.5}\text{MnO}_3$  (right) at room temperature. Fundamental diffraction spots are shown with numbers, and superlattice spots from CO are indicated with arrows. (c) The magnetic susceptibility measured at 100 K.

different from those of  $Pnma$ -type. The absence of (100)- or (001)-type spots in the patterns indicate that the structure is close to tetragonal, such as  $Imma$ . In addition to this difference in fundamental peaks, the superlattice peaks for  $x = 0.35$  and  $0.5$  indicate a different CO scheme with incommensurate wave vector,  $\mathbf{q} = (1/2 - \delta)\mathbf{a}^*$ , where  $\delta$  measures the incommensurability. We found that  $\delta$  varies slightly in different crystallites. The range of measured  $\delta$  in different regions is shown in Fig. 3(b) with the average  $\delta$  value. Note that the results of our high-resolution TEM experiments on  $\text{Bi}_{0.5}\text{Sr}_{0.5}\text{MnO}_3$  showed that the lattice-fringes with  $2.8 \text{ \AA}$  ( $\cong a/2$ ) spacing for the DS-type CO shifts occasionally due to the presence of antiphase boundaries, and that the spacing between these boundaries is about  $20a$  ( $110 \text{ \AA}$ ), indicating that the incommensurability with  $\delta \cong 0.06$  is of a discommensuration-type. We note that no significant temperature dependence was found down to 90 K. The magnetic susceptibility at 100 K with  $x$  exhibits a behavior similar with that of  $\delta$  [Fig. 3(c)], suggesting that magnetic susceptibility increases with increasing incommensurability. It is worthy to note that this amount of  $\delta$  is enough to result in phase-separation or ferromagnetism in the CB-type  $\text{La}_{0.5}\text{Ca}_{0.5}\text{MnO}_3$ .<sup>2,6,15</sup> The smooth evolution of volume across the structural phase boundary in  $\text{Bi}_{0.5}(\text{Ca},\text{Sr})_{0.5}\text{MnO}_3$  probably indicates the nature of

$\text{Bi } 6s^2$  lone pairs does not change across the structural phase boundary, so this may not be an important consideration for the different CO schemes found in  $\text{Bi}_{0.5}(\text{Ca},\text{Sr})_{0.5}\text{MnO}_3$ . However, the strong localization tendency of charge carriers in  $\text{Bi}_{0.5}(\text{Ca},\text{Sr})_{0.5}\text{MnO}_3$  is probably related with the presence of  $\text{Bi } 6s^2$  lone pairs, which may be randomly frozen in the perovskite A-sites, inducing random local structural distortions. The difference between  $\text{Bi}_{0.5}\text{Ca}_{0.5}\text{MnO}_3$  and  $\text{Bi}_{0.5}\text{Sr}_{0.5}\text{MnO}_3$  may result from the different chemical pressure or tolerance factor. For example, in the case of  $\text{Bi}_{0.5}\text{Sr}_{0.5}\text{MnO}_3$  with large Sr ions, large local Jahn–Teller structural distortions around Mn ions can be accommodated while the small tolerance factor associated with Ca ions induces uniform distribution of Jahn–Teller distorted regions. Evidently the subtle interplay among  $\text{Bi } 6s^2$  lone pairs, Jahn–Teller distortion around  $\text{Mn}^{3+}$  ions, and tolerance factor plays a crucial role in fixing the CO pattern in Bi-based half-doped manganites.

#### 4. Conclusions

In conclusion, the phase diagram of  $\text{Bi}_{0.5}\text{Ca}_{0.5-x}\text{Sr}_x\text{MnO}_3$  exhibits a bicritical nature of two types of CO ground states, indicating the immiscibility as well as competition between these CO phases. CO in  $\text{Bi}_{0.5}\text{Sr}_{0.5}\text{MnO}_3$ , maintaining the Jahn–Teller characteristics of  $\text{LaMnO}_3$ , turns out to be robust against thermal and chemical fluctuations. Our results suggest that the DS-type CO in  $\text{Bi}_{0.5}\text{Sr}_{0.5}\text{MnO}_3$  can be stabilized by a large tolerance factor associated with Sr ions through accommodating the local lattice distortions due to  $\text{Bi } 6s^2$  lone pairs and Jahn–Teller Mn ions.

- 1) E. J. W. Verwey: *Nature (London)* **144** (1939) 327.
- 2) C. H. Chen and S.-W. Cheong: *Phys. Rev. Lett.* **76** (1996) 4042.
- 3) C. H. Chen, S.-W. Cheong, and H. Y. Hwang: *J. Appl. Phys.* **81** (1997) 4326.
- 4) P. G. Radaelli, D. E. Cox, M. Marezio, and S.-W. Cheong: *Phys. Rev. B* **55** (1997) 3015.
- 5) S. Mori, C. H. Chen, and S.-W. Cheong: *Nature (London)* **392** (1998) 473.
- 6) S. Mori, C. H. Chen, and S.-W. Cheong: *Phys. Rev. Lett.* **81** (1998) 3972.
- 7) R. Wang, J. Gui, Y. Zhu, and A. R. Moodenbaugh: *Phys. Rev. B* **61** (2000) 11946.
- 8) P. M. Woodward, T. Vogt, D. E. Cox, A. Arulraj, C. N. R. Rao, P. Karen, and A. K. Cheetham: *Chem. Mater.* **10** (1998) 3652.
- 9) J. L. García-Muñoz, C. Frontera, M. A. G. Aranda, A. Llobet, and C. Ritter: *Phys. Rev. B* **63** (2001) 064415; C. Frontera, J. L. García-Muñoz, M. A. G. Aranda, A. Llobet, M. Respaud, and J. Vanacken: *Phys. Rev. B* **64** (2001) 054401; C. Frontera, A. Llobet, M. A. G. Aranda, C. Ritter, and J. L. García-Muñoz: *Physica B* **276–278** (2000) 793.
- 10) R. D. Shannon: *Acta Crystallogr., Sect. A* **32** (1976) 751.
- 11) M. Hervieu, A. Maignan, C. Martin, N. Nguyen, and B. Raveau: *Chem. Mater.* **13** (2001) 1356.
- 12) G. Subias, J. Garcia, P. Beran, M. Nevriřva, M. C. Sanchez, and J. L. Garcia-Munoz: *Phys. Rev. B* **73** (2006) 205107.
- 13) W. Bao, J. D. Axe, C. H. Chen, and S.-W. Cheong: *Phys. Rev. Lett.* **78** (1997) 543.
- 14) S. Sachdev: *Science* **288** (2000) 475; J. Burgy, M. Mayr, V. Martin-Mayor, A. Moreo, and E. Dagotto: *Phys. Rev. Lett.* **87** (2001) 277202.
- 15) R. Shoji, S. Mori, N. Tamamoto, A. Machida, T. Moritomo, and T. Katsufuji: *J. Phys. Soc. Jpn.* **70** (2001) 267.